Energy 76 (2014) 788–798

Contents lists available at ScienceDirect

Energy

journal homepage: www.elsevier.com/locate/energy

A study of using a thermoelectric generator to harvest energy from a table lamp

Chien-Chou Weng, Mei-Jiau Huang*

Department of Mechanical Engineering, National Taiwan University, Taipei 106, Taiwan

ARTICLE INFO

Article history:
Received 19 February 2014
Received in revised form
21 August 2014
Accepted 22 August 2014
Available online 17 September 2014

Keywords:
Lamp
Waste heat recovery
Thermoelectric generator
Compact heat sink model

ABSTRACT

The application of a TEG (thermoelectric power generator) to harvest energy from the waste heat of a commercial table lamp was investigated experimentally as well as numerically. The table lamp was integrated with TEG chips which were cooled by a natural convection heat sink. In the simulation, the heat sink was not truly simulated but modeled by the compact heat sink model. The effective thermal conductivity of the fiction fluid in the compact model was calibrated by matching the calculated and measured temperatures. A 1D TEG model taking the Peltier and Joule heats into consideration was then proposed to predict the power generation rate based on the simulated hot side and cold side thermal conductances of the open-circuit system. The prediction is in a good agreement with the closed-circuit simulation results but has a slightly larger maximum power generation rate and a slightly smaller optimal electric load than the experimental measurements. It was attributed to the effect of the remaining electric resistances in the circuit other than the internal resistance of the TEG chips and external load. Finally, it was found that the low hot-side thermal conductance is the main reason for the low power generation efficiency.

1. Introduction

Nowadays, lighting is essential in daily life. An important fraction of the total electricity consumed worldwide attributes to the electricity used for lighting system: 5~15% of the national electricity consumption in the industrialized countries and higher than 80% in some developing countries [1]. In 2005, there were more than 33 billion lamps worldwide, consuming annually about 2650 TWh of electricity which was as much as 19% of total global electricity consumption [1,2]. According to [3,4], the heat dissipation factors of the lamps are very high: 95% of input power for incandescent lamps, 73~77% of input power for compact fluorescent lamps, and 87~90% of input power for high-brightness LEDs. That means the vast majority of energy is wasted as heat. Suppose the heat dissipation factors of all the lamps in 2005 are 0.75, about 2000 TWh of energy are wasted. If this energy could be recovered, it would be helpful to the energy crisis that the earth is facing now. For instance, Rubén [5] proposed a water-cooled-heat-sink assembly to recover waste heat from luminaries, lamps and LED devices; the heated water can be reused for domestic water heating.

Thermoelectric power generators are good for recovering energy from the waste heat because they can directly transfer heat to electrical energy and have the advantages of light weight, no noise, and no mechanical vibration. Because of the environmental protection issues and energy crisis, TEG (thermoelectric power generator) applications have been extensively studied in recent decades, such as in wearable electronic products, gas sensors, automobiles, wood stoves, geothermal energy systems, solar energy systems, etc [6–13]. The wearable electronic products, such as watches and electronic medical instruments, can be driven by human-body TEGs [7]. Matsumiya et al. [8] proposed a thermoelectric CO gas sensor to detect the target gas content by the voltage signal produced by the temperature raise due to the catalytic reaction oxidation of CO. Champier et al. [9] added TEGs to a multifunction wood stove and obtained a maximum stabilized electrical power of 7.6 W for the end users. Hsu et al. [10] proposed a heat exchanger with a slopping block in the inlet to harvest waste heat from the automotive exhaust pipe and obtained a maximum power of 12 W. Weng and Huang [11] designed and simulated a heat exchanger attached with TEGs for recovering waste heat from the automotive exhaust pipe; it was revealed that implementing more TEGs may not necessarily produce more power because the heat sinks attached to the downstream TEGs may loot heat from the upstream hotter wall, resulting in a performance degradation of the

* Corresponding author. Tel.: +886 2 33662696; fax: +886 2 23631755.
E-mail address: mjhuang@ntu.edu.tw (M.-J. Huang).

http://dx.doi.org/10.1016/j.energy.2014.08.078
0360-5442/

upstream TEGs. Suter et al. [12] established a heat transfer model to optimize a 1 kW geothermal TEG for either a maximum conversion efficiency or a minimum volume of the system. Chen [13] investigated the optimal performance of a STEG (solar thermoelectric generator); the maximum power generation rate and the optimal electric load were analyzed. It was also found that the optimal electric load is larger than the internal electric resistance of the STEG as also noticed in Ref. [14]. In fact, the optimal electric load associated with the maximum power is equal to the internal electric resistance of the TEG chips only when the TEG chips alone are analyzed. However, when the overall system is concerned, the optimal electric load would be larger than the internal electric resistance of the TEG chips due to the finite thermal conductances between the hot side of the TEG chips and the heat source and between the cold side of the TEG chips and the heat sink [13].

In order to accurately optimize the energy harvesting system, the interactions between the TEG chips and the heat source/sink should be considered. Both system models [12–17] and simulation methods [18,19] have developed to include this issue in the system analysis. Liang et al. derived an approximate analytical solution of the power generation rate from a 1D TEG model [14] with the TEG chips electrically connected in series [15] or in parallel [16]. In these studies, each TEG chip has its own heat source and heat sink, and the heat transferred between the TEG chips is ignored. Astrain et al. [17] studied how the thermal resistances of the heat exchangers influence the maximum power of a TEG and coupled this model with Fluent to estimate the maximum harvesting energy from the smoke produced by a combustion boiler in a paper mill. ANSYS Inc. [18] provides a set of ANSYS coupled-field elements and enables users to analyze thermoelectric devices by solving the energy equation and the continuity equation of the electric charge based on the finite element method within every TE leg and the copper strap of a TEG chip. Chen et al. [19] developed their own 3D algorithm for both the thermal field and the electric field and incorporated it with the ANSYS-Fluent through a finite volume method numerical scheme. These simulation methods can provide detailed information and are very useful for designing TEG chips. However these methods are complicated and computationally time-consuming.

So far, not many studies have been performed for the waste heat recovery from the lamps by using a TEG. Simon et al. [20] proposed recycling the LED waste heat by a TEG to increase the efficiency of the LEDs. YAMAHA developed a TEG system to recover waste heat from the projector lamp; a system efficiency of 3.2% was achieved experimentally by using a TEG chip which conversion efficiency is 5.6% as the temperature difference is 150 K [21]. More researches are still needed to further understand the lamp waste heat recovery system, such as the exact amount of energy that can be possibly recovered, the reasons behind the unsatisfactory efficiency, new designs for efficiency enhancement, etc. In this work, for the first time to the authors' knowledge, a complete lamp-TEG system including two lamp tubes, the lampshade, the reflector, the TEG chips, and so on is analyzed. Such a lamp-TEG system was built and studied experimentally as well as numerically. The simulations were performed by using the commercial software ANSYS-Fluent. Both open-circuit and closed-circuit systems were simulated. To avoid the difficulties associated with the simulation of the closed-circuit system, we propose a 1D model which can count the thermoelectric effects in predicting the power generation rate based on the simulation results of the open-circuit system. The accuracy of the model prediction will be examined. Finally, applications with two TEG chips connected electrically in series as well as in parallel were investigated and compared.

The rest of this paper introduces the experimental setup and the simulation model in Sections 2 and 3 respectively, presents the results and discussions in Section 4, and finally gives the conclusions in Section 5.

2. Experiment setup

The commercial table lamp studied herein consists of a 13 W non-integrated compact fluorescent lamp, a black-ABS-plastic lampshade, and an aluminum reflector as shown in Fig. 1. The fluorescent lamp has two lamp tubes of diameter 13 mm and length 139.5 mm. The lampshade looks like a half-round-nose bullet of length 272 mm and base diameter 62 mm. The lamp cap is 10 mm long. In order to mount the TEG chips on the top of the reflector, we dug a 40 mm × 140 mm hole on the lampshade above the fluorescent lamp. The U-bend reflector is made of an aluminum sheet of thickness 0.8 mm, length 150 mm, and width 85.7 mm. In the present study, a TEG chip (TGM-199-1.4-1.5, Kryotherm) composed of 199 TE couples was employed. Its overall dimensions are 40 mm in length, 40 mm in width, and 3.9 mm in height. The effective Seebeck coefficient (α) and the effective internal electric resistance (R_{TEG}) of the TEG chip are 0.0612 V/K and 2.54Ω respectively. The effective Seebeck coefficient is defined as the ratio of the induced open-circuit voltage to the temperature difference between the two ceramic plates of the TEG chip; the effective internal electric resistance includes the electric resistances of the TE legs and the copper strap as well as the in-between electric contact resistances. A natural-convection heat sink is attached to the TEG chips. A 45 mm × 45 mm × 30.5 mm heat sink with 5 fins was employed for the one-TEG-chip system (Fig. 1a) and a 102 mm × 51 mm × 22 mm one with 8 fins was employed for the two-TEG-chips system (Fig. 1b). Finally, in order to prevent the heat loss from the bottom of the lampshade, an acrylic sheet was added below the lamp tubes. With the acrylic sheet, the surface temperature of the fluorescent lamp is raised by about 10 °C.

The experimental procedures are described as follows. The air conditioner was turned on first to maintain the room temperature at 300 K. We turned on the lamp next and waited for at least 40 min for the system to reach steady before the temperatures of the lamp-TEG system were measured. The voltage across the external electric load was then measured with the external electric load increased stepwise. The experiment was repeated three times for each system and each time the experiment wouldn't start unless the system had been completely cooled down after the lamp was turned off. The temperature was measured by the K-type thermometer with a resolution of 0.1 °C and an accuracy of 0.1% + 0.7 °C in the range of −100 °C~200 °C. The external load and the voltage across it were measured by a 3-1/2 multimeter with a resolution of 0.1 Ω and 1 mV and an accuracy of 2%+2 dgt and 0.5%+1 dgt respectively. Take one example. Suppose we read 6.0 Ω and 80 mV from the 3-1/2 multimeter, the measurement errors of the resistance and the voltage are ±0.32 Ω and ±1.4 mV (±1.8%) respectively. The error associated with the power generation rate therefore is 0.094 mW (±9%).

3. Simulation and 1D TEG model

3.1. Simulation model

The energy recovery system built in the previous section was also simulated. The simulation model is illustrated in Fig. 2. The system is assumed to be symmetric with respect to the plane of $y = 0$ and thus a simulation of half the system is sufficient. The overall simulation domain has a dimension of [−440,710] × [0,500] × [−500,600] in millimeter. The lamp tubes are aligned with the x axis and the origin of the coordinate system is located on the base-surface of the lampshade. In the simulation, the

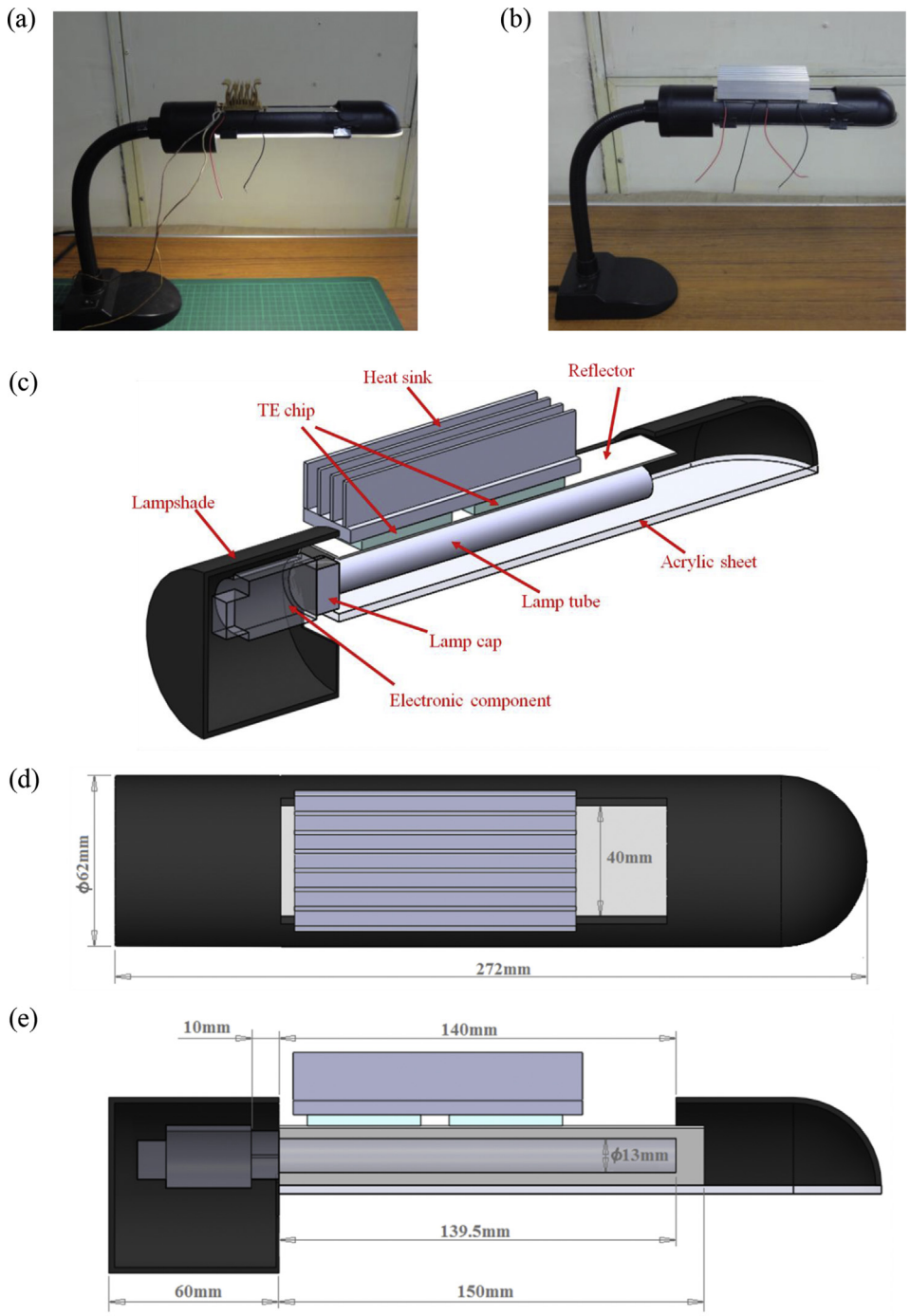

Fig. 1. The lamp energy recovery system: (a) mounted with one TEG chip cooled by a small heat sink, (b) mounted with two TEG chips cooled by a large heat sink, (c) the schematic diagram of the two-TEG-chips system, (d) the dimensions on the top view, (e) the dimensions on the front view.

lampstand and electronic component are neglected. Each TEG chip is modeled as a cuboid of thickness 3.9 mm and base area 40 mm × 40 mm with a thermal conductivity of 2.68 W/m-K, corresponding to a thermal conductance (K_{TEG}) of 1.10 W/K as supplied by the TEG-chip manufacture. The surrounding of the system is full of air whose properties (density, thermal diffusivity, and the momentum diffusivity) vary with temperature. The thermal conductivities of the ABS lampshade, the acrylic sheet, the reflector, and the base plate of the heat sink are set to be 0.18 W/m-K [22], 0.21 W/m-K [22], 120 W/m-K, and 202 W/m-K respectively. The heat sink on the top of the TEG chip is modeled by the so-called compact heat sink model as described below.

3.2. Compact heat sink model

The compact heat sink model [23–25] replaces the fins above the base plate of the heat sink by a finite volume of some fiction fluid which thermal and flow resistances are equivalent to those of the actual heat sink. The flow resistance is minor in the present application because the pressure drop caused by the buoyancy-

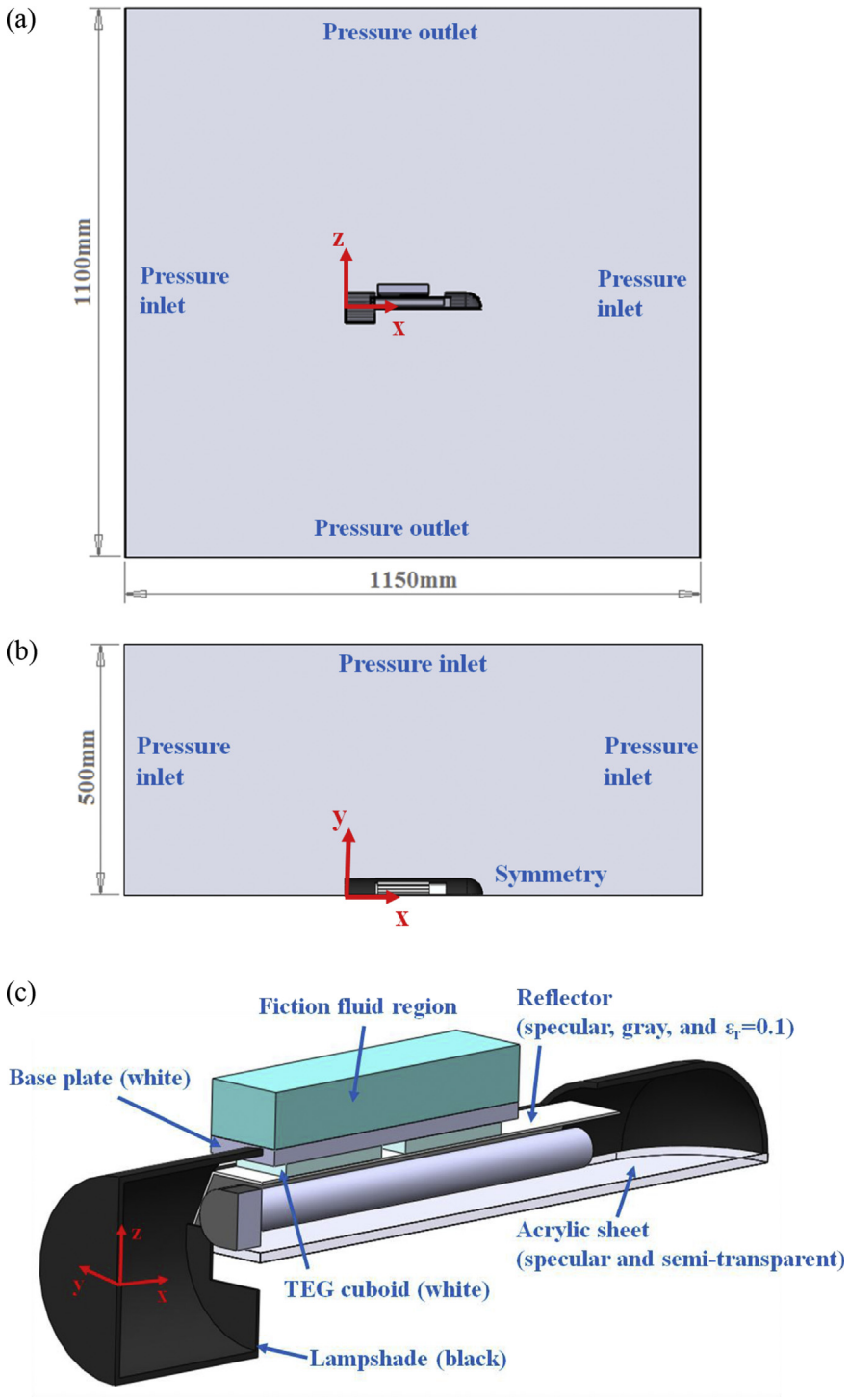

Fig. 2. (a) The front view and (b) the top view of the simulation domain with the employed boundary conditions indicated, (c) the simulation model and radiative properties employed in this study.

driven current is small. A viscosity as the same as that of the ambient air is thus assumed. The effective thermal conductivity of the fiction fluid is in general determined by the known thermal resistance of the actual heat sink and an appropriate Nusselt number correlation [26]. However, because we are short of such information, we retain the effective thermal conductivity of the fiction fluid as a free parameter and calibrate it by matching the simulation results with the experimental data.

3.3. Simulation method

An unstructured mesh system composed of about 6×10^6 elements was carefully built. The unstructured mesh was employed herein because there are many components in the system and most of them have irregular complex geometries. A structured mesh must result in a high mesh-skewness, which in turn results in instability and poor accuracy. Fig. 3 shows the grid configuration.

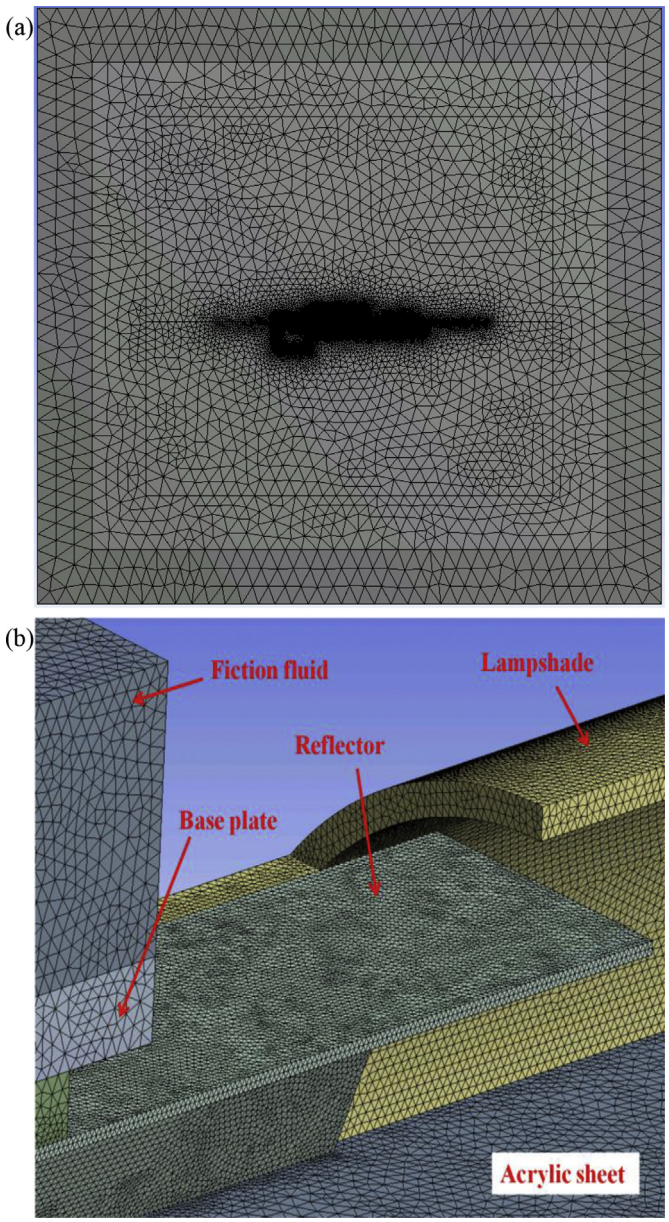

Fig. 3. The medium grid configuration: (a) the front view of the whole computational domain and (b) some parts of the lamp-TEG model.

For every thin component in the system except the reflector and some parts of the lampshade, we used at least three grid points across the thickness. The average skewness is 0.23 and the maximum skewness is 0.94. The SIMPLE algorithm and first-order upwind scheme were chosen to solve the steady-state laminar natural convection and radiation problem. The DO (discrete ordinates) method, in which radiation intensities along some preselected directions at each grid point are calculated, was adopted for solving the radiative transfer equation [27]. In the simulation, the radiation was considered in all the fluid regions and within the acrylic sheet, the number of discrete solid angles was 32, and no absorption and scattering was considered. Ignoring the absorption and scattering of air results in more radiation heat transfer between the lamp-TEG system and the environment. Ignoring the absorption and scattering of the acrylic sheet may reduce the temperature of the acrylic sheet on the other hand. However, the influence is negligible because the air has extremely low absorptivity and the sheet is very thin. The refractive indices of air and the acrylic sheet are 1 and 1.49 respectively. The gravity, $g = 9.81\ m^2/s$, is directed toward the negative z direction in the simulation. No buoyancy-driven flow model was adopted in this study. The buoyancy force arises naturally when there is a temperature difference and the gravity is existent, because all the air properties including the density are temperature-dependent. The convergence criteria adopted were a scaled residual under 10^{-3} for the mass balance, 10^{-5} for the momentum balance, and 10^{-10} for the energy balance.

The no-slip boundary condition was imposed at all the solid walls. The ambient pressure and temperature were 1 atm and 300 K respectively. The ambient temperature set to 300 K because the experiments were operated at a room temperature of 300 K, a room temperature that occurs quite often in daily life. The pressure inlet boundary condition (a total pressure of 1 atm, 300 K, and zero tangential velocity components) was imposed at the lateral boundaries of the computational domain. Imposed at the top and bottom boundaries of the computational domain was the pressure outlet boundary condition: a static pressure of 1 atm and all other flow quantities extrapolated from the interior domain. These boundary conditions were determined because the flow is induced purely by the buoyancy force in the central part of the computational domain and the flow is mainly upward. We attempted other boundary conditions as well and found this one results in the most reasonable flow pattern. Note that the boundary conditions employed do not replicate the experiment completely, because there are many other objects in the real world such as the lamp stand, the desk/floor, and so on, which are not taken into consideration in the simulation. The measured steady temperatures of the lamp tube and the lamp cap (see Fig. 4) were imposed as part of the boundary conditions in the simulation as well. As far as radiation is concerned, the surfaces of the acrylic sheet are specular and semi-transparent, the surfaces of the TEG cuboid and the base plate of the heat sink are white, the surface of the reflector having an emissivity $\varepsilon_r = 0.1$ (the emissivity of the aluminum surface is about 0.09 for commercial aluminum sheet at 400 K [28]) is specular and gray, and finally all the other surfaces are black.

3.4. 1D TEG model

For simplicity, the open-circuit system is usually simulated. A direct use of the so-obtained steady temperature difference

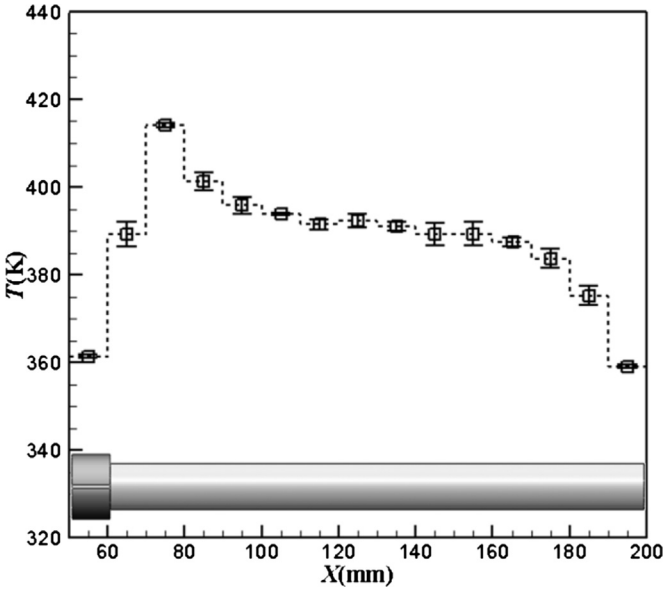

Fig. 4. The temperature distribution of the lamp tube.

(ΔT_{open}) between the hot and cold sides of the TEG cuboid however results in an overestimated power generation rate for a given electrical load (R_{load}), because the influence of the Peltier and Joule heats is not counted. To fix it, we propose herein a 1D TEG model which takes these heats into account. In Fig. 5, K_H is the thermal conductance between the heat source and the hot side of the TEG chips and K_C is the thermal conductance between the cold side of the TEG chips and the ambiance. The heat transferred to the TEG chips (Q_H) and the heat dissipated from the TEG chips to the heat sink (Q_C) can therefore be expressed as

$$Q_H = K_H(T_S - T_H) \tag{1}$$

$$Q_C = K_C(T_C - T_a) \tag{2}$$

where T_H and T_C are the hot-side and cold-side temperatures of the TEG chip, T_S is the temperature of the heat source, and T_a is the ambient temperature. On the other hand, it is well-known that Q_H and Q_C can also be expressed as follows:

$$Q_H = N\alpha I T_H + NK_{TEG}\Delta T - \frac{N}{2}I^2R_{TEG} \tag{3}$$

$$Q_C = N\alpha I T_C + NK_{TEG}\Delta T + \frac{N}{2}I^2R_{TEG} \tag{4}$$

with

$$I = N\alpha\Delta T/(NR_{TEG} + R_{load} + R_c) \tag{5}$$

for N identical TEG chips electrically connected in series, or

$$I = \alpha\Delta T/[R_{TEG} + N(R_{load} + R_c)] \tag{6}$$

for N identical TEG chips electrically connected in parallel. In the above equations, I is the electric current through a TEG chip, ΔT ($=T_H - T_C$) is the temperature difference across the TEG chip, and R_c is the remaining electric resistance, such as the electric resistances of the electric wires and the electric contact resistances at joins of electronic components in the electric circuit. Eqs. (1)–(6) provide a basis for a calculation of ΔT as a function of R_{load} as long as T_S, T_a, K_H, K_C, and R_c are known. The exact solution of Eqs. (1)–(6) can be easily obtained numerically. The power generation rate can then be calculated by

$$P = I^2R_{load} \tag{7}$$

for TEG chips electrically connected in series, and

$$P = (NI)^2R_{load} \tag{8}$$

for TEG chips electrically connected in parallel.

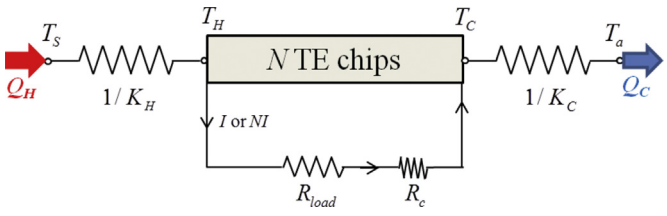

Fig. 5. An illustration of the 1D TEG model. The electric current through the electric load is I for the series network and NI for the parallel network.

Table 1
The information and the simulation results of the three grid configurations.

	Sparse grid	Medium grid	Dense grid
The number of meshes	2×10^6	6×10^6	12×10^6
The number of meshes across the thickness of the reflector	1	2	3
The number of meshes across the thickness of the lampshade	2	3	4
The average top-surface temperature over the middle line of the reflector	332.35 K	332.23 K	332.16 K
The average top-surface temperature over the middle line of the lampshade	309.57 K	309.47 K	309.47 K

In this study, $T_S = 385.63$ K is the average temperature of the lamp tubes and the lamp cap and $T_a = 300$ K. We propose herein to extract K_H and K_C from the open-circuit simulation, calculated as

$$\frac{1}{K_H} = \frac{T_S - T_{H,open}}{Q_{H,open}} \tag{9}$$

$$\frac{1}{K_C} = \frac{T_{C,open} - T_a}{Q_{C,open}} \tag{10}$$

where T_H and T_C are taken as the averaged temperatures over the hot-side and cold-side surfaces of all the TEG cuboids respectively, and the subscript "open" represents a value extracted from the open-circuit simulation.

3.5. Peltier and Joule heats

Closed-circuit simulations were also performed in order to confirm the accuracy of the 1D TEG model described in the previous subsection. The methods proposed by ANSYS Inc. [18] and Chen et al. [19] for the sake of taking the thermal-electric coupled effect into consideration are not adopted in this study, because the design of the TEG chip itself is not the purpose of this study. A UDF program is coded instead to incorporate the thermal-electric effect in the following way. Firstly, the Joule heat is treated as an additional volumetric heat source uniformly distributed within the TEG cuboids. Thomson heat is ignored because of the low temperature difference between the hot and cold sides of the TEG chip in the present application. A heat sink of strength $-\alpha I_i T_{H,i}$ and a heat source of strength $\alpha I_i T_{C,i}$ are added at the hot-side and cold-side surfaces respectively of the ith TEG cuboid to model the Peltier effect, where $T_{H,i}$ and $T_{C,i}$ are the averaged temperatures over the hot-side and cold-side surfaces of the ith TEG cuboid respectively. The electric current flowing through the ith TEG chip, namely I_i, is coupled to the temperature difference $\Delta T_i \equiv T_{H,i} - T_{C,i}$ by

$$I_i = \sum_{i=1}^{N} \alpha\Delta T_i/(NR_{TEG} + R_{load} + R_c) \tag{11}$$

when TEG chips are electrically connected in series, and by

$$I_i = \frac{\alpha\Delta T_i}{R_{TEG}} - \sum_{j=1}^{N} I_j \cdot \frac{R_{load} + R_c}{R_{TEG}} \tag{12}$$

when TEG chips are electrically connected in parallel. An iteration is obviously required for a convergence of the induced currents I_i's and the closed-circuit temperature differences ΔT_i's.

4. Result and discussion

4.1. Verification of the simulation method

Before simulating the energy recovery system, a lamp model without the TEG chip and the attached heat sink was simulated first to verify the validity of the grid and the simulation model. Three spatial resolutions were attempted, the sparse, medium, and dense ones. The information of these three grid configurations and their test results were listed in Table 1. The average top-surface temperatures over the middle line of the reflector and the lampshade (the black dash lines indicated in Fig. 6) were compared. As shown in Table 1, the results are nearly the same, especially those from the medium grid and the dense grid. Therefore all the following simulations were performed based on the medium grid configuration.

Fig. 6 shows the temperature distribution on the solid surfaces. The acrylic sheet has a higher temperature and a larger temperature gradient than the reflector due to its lower thermal conductivity. The surface temperature distribution along the middle lines of the top surfaces of the lampshade and the reflector is shown in Fig. 7, compared with the experimental measurements. It is observed that the simulated temperatures of the reflector and the left lampshade are close to the measured ones but that of the right lampshade is slightly overestimated. It is because the real lampshade is not a black body. This overestimate is not observed in the left lampshade because it is seemingly redeemed by the neglect of the electronic component in the simulation. A total of waste heat of 10.02 W (including 4.93 W radiation heat) dissipated into the ambient air is found from the simulation, which is about 78% of input power (13 W), close to the heat dissipation factor (73%~77%) of a commercial compact fluorescent lamp. As a whole, the simulation result is in a good agreement with the experimental measurement and therefore the validity of the simulation model is verified.

4.2. The lamp waste heat recovery system

Two open-circuit systems are simulated. One is mounted with one TEG chip cooled by a small heat sink (Fig. 1a), and the other is mounted with two TEG chips cooled by a large heat sink (Fig. 1b). The small heat sink is modeled as a combination of a 45 mm × 45 mm × 1.5 mm base plate and a fiction-fluid region of 45 mm × 45 mm × 29 mm, and the large heat sink is modeled as a combination of a 102 mm × 51 mm × 5 mm base plate and a fiction-fluid region of 102 mm × 51 mm × 17 mm. Three different effective thermal conductivities (k_e) for the fiction fluid are attempted for each system, and the simulation results of the open-circuit systems are summarized in Table 2. Substituting the computed thermal conductances, $K_{H,\text{open}}$ and $K_{C,\text{open}}$, into the 1D TEG model, the power generation rate as $R_c = 0\ \Omega$ is shown in Fig. 8; the one predicted by a direct use of the open-circuit temperature difference as the ΔT in Eq. (5) or (6) is also plotted for comparison. It shows that the power generation rate becomes smaller and the optimal electric load for the maximum power becomes larger under the influences of the Peltier and Joule heats. Fig. 9 shows the hot-side and cold-side temperatures and the temperature difference of the TEG cuboid calculated from the 1D TEG model against the electric load. The temperature difference should approach to the open-circuit temperature difference (2.1 K) as the electric load becomes huge (the electric current and consequently the Peltier as well as Joule heats become extremely small). As the electric load decreases, a larger electric current is generated and so are the Peltier heats at both the hot and the cold sides of the TEG chip. Consequently T_H is slightly decreased and T_C is slightly increased; the net effect is a decreasing temperature difference. This explains why $\Delta T_{\text{closed}} < \Delta T_{\text{open}}$.

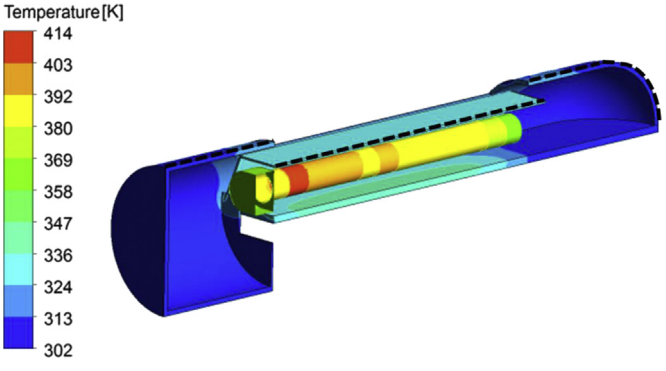

Fig. 6. The temperature distribution on the solid surfaces of the lamp model without the TEG chip and the heat sink.

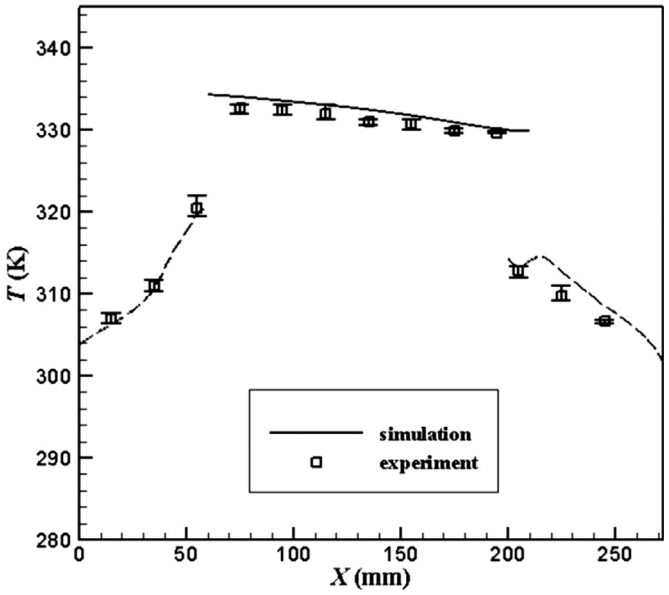

Fig. 7. The simulated surface temperature along the middle lines of the top surfaces of the lampshade (dash line) and the reflector (solid line), compared with the experimental measurements (symbols).

The simulation results of the closed-circuit systems are listed in Table 3 and also shown in Figs. 8 and 9, when the electric load is equal to the equivalent electric resistance of the TEG-chip network (NR_{TEG} for the series network and R_{TEG}/N for the parallel network), that is the optimal electric load under fixed T_H and T_C. The results agree excellently with the predictions of the 1D TEG model. One of the reasons for the agreement is that $K_{H,\text{closed}}$ and $K_{C,\text{closed}}$ are

Table 2
The simulation results of the open-circuit systems.

k_e (W/m-K)	Q_H (W)	T_H (K)	$1/K_H$ (K/W)	Q_C (W)	T_C (K)	$1/K_C$ (K/W)
(a) The system with one TEG chip						
2	1.92	321.82	33.27	1.90	320.09	10.59
4	2.14	320.20	30.53	2.13	318.26	8.59
10	2.32	318.89	28.72	2.31	316.78	7.27
(b) The system with two TEG chips						
1	2.85	319.70	23.10	2.83	318.41	6.50
2	3.08	318.32	21.84	3.06	316.92	5.53
4	3.21	317.52	21.20	3.19	316.06	5.03

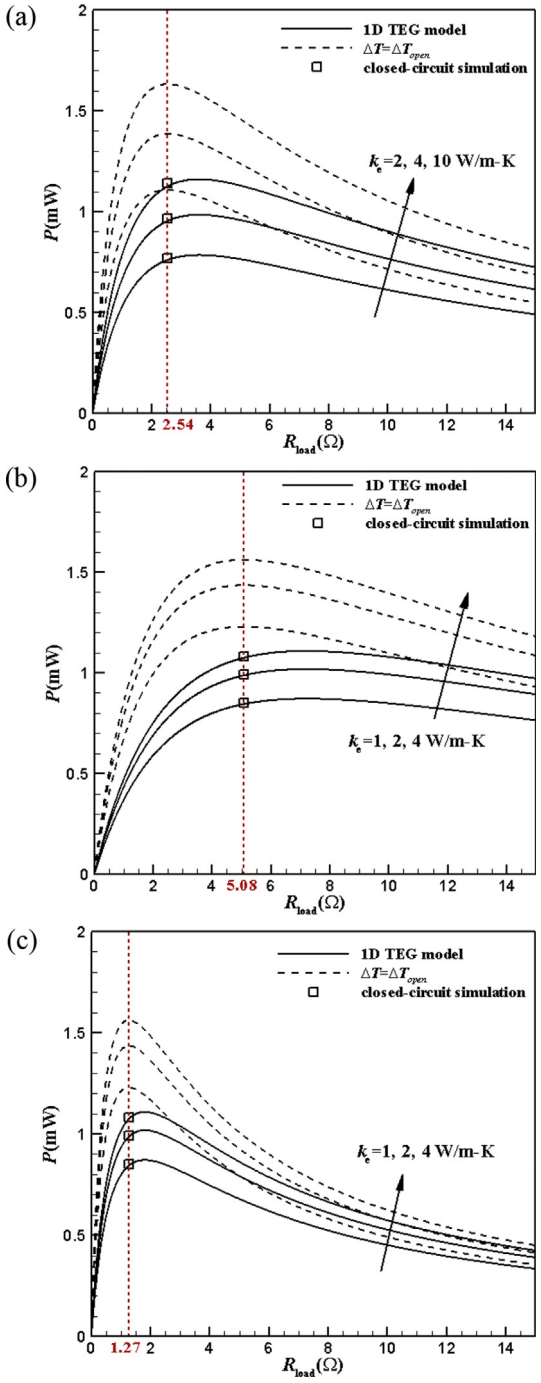

Fig. 8. The simulated/predicted power generation rate of the lamp energy recovery system against the electric load. (a) one TEG chip mounted, (b) two TEG chips connected electrically in series, (c) two TEG chips connected electrically in parallel.

almost as the same as $K_{H,\text{open}}$ and $K_{C,\text{open}}$. The other reason is the heat loss from the lateral surfaces of the TEG cuboids ($Q_H - Q_C - P$), which is not considered in the 1D model but appears in the simulation, is relatively small, compared with the heat transferred to the TEG cuboids (Q_H). In the open-circuit simulation with one TEG chip and $k_e = 10$ W/m-K, this heat loss is only 0.5% of Q_H. In other words, the agreement may not be good if the temperature difference of the system is large or the Peltier heat and Joule's heat are huge because a consideration of these heats or not may result in significantly different thermal-flow fields in the neighborhoods of

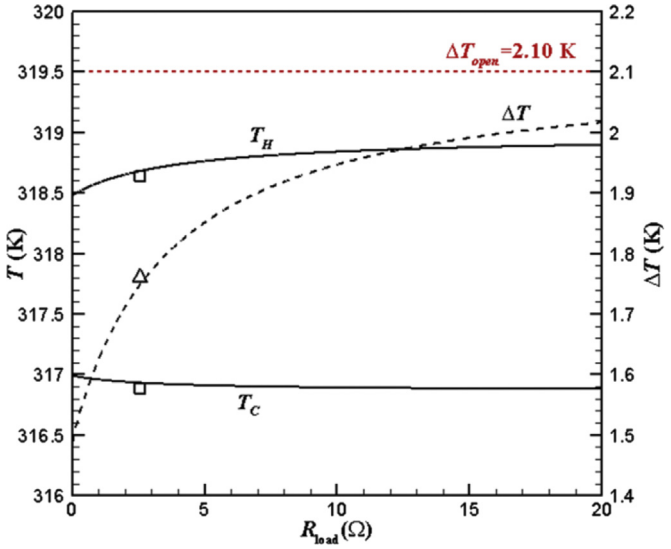

Fig. 9. The predicted hot-side and cold-side temperatures of the TEG cuboid and the temperature difference (dash line) against the electric load for the one-TEG-chip system based on the open-circuit simulation with $k_e = 10$ W/m-K. Symbols (□ and △) indicate the temperatures and temperature difference from the closed-circuit simulation.

the cold and hot sides of the TEG chips. That means the difference between $K_{H,\text{closed}}$ ($K_{C,\text{closed}}$) and $K_{H,\text{open}}$ ($K_{C,\text{open}}$) possibly increases with increasing temperature difference. In remark, the 1D TEG model combined with the open-circuit simulation does a good job in predicting the power generation rate at least in low temperature-difference applications. In such a way, closed-circuit simulations are successfully avoided.

4.3. Experimental measurement

The middle-line temperatures on the top surfaces of the lampshade and the reflector in the open-circuit system are measured by the K-type thermocouples and shown in Fig. 10, compared with the open-circuit simulation results. As observed in Section 4.1, the measured temperature of the left lampshade is close to the simulation one but that of the right lampshade is lower. The measured temperature data of the reflector are distributed between the simulation results of $k_e = 4$ W/m-K and $k_e = 10$ W/m-K in the one-TEG-chip system and close to the simulation result of $k_e = 2$ W/m-K in the two-TEG-chips system. The reflector temperature at $x = 115$ mm of the one-TEG-chip system slightly deviates from the

Table 3
The simulation results of the closed-circuit systems.

k_e (W/m-K)	Q_H (W)	T_H (K)	$1/K_H$ (K/W)	Q_C (W)	T_C (K)	$1/K_C$ (K/W)
(a) The system with one TEG chip and $R_{load} = R_{TEG} = 2.54\Omega$						
2	1.94	321.65	32.93	1.92	320.20	10.51
4	2.17	319.98	30.21	2.15	318.36	8.52
10	2.36	318.64	28.41	2.34	316.88	7.21
(b) The system with two TEG chips electrically connected in series and $R_{load} = 2R_{TEG} = 5.08\Omega$						
1	2.88	319.55	22.94	2.86	318.48	6.47
2	3.11	318.15	21.69	3.09	316.99	5.50
4	3.25	317.33	21.05	3.23	316.12	5.00
(c) The system with two TEG chips electrically connected in parallel and $R_{load} = R_{TEG}/2 = 1.27\Omega$						
1	2.88	319.55	22.94	2.86	318.48	6.47
2	3.11	318.15	21.69	3.09	316.99	5.50
4	3.25	317.33	21.04	3.23	316.12	5.00

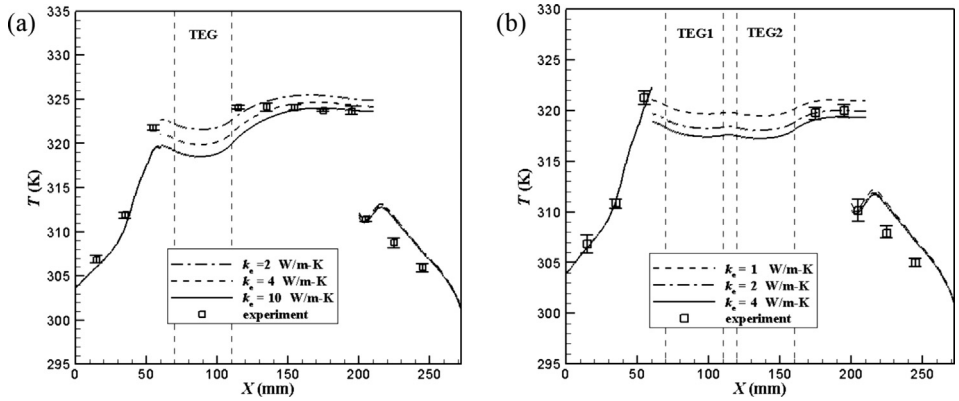

Fig. 10. The middle-line temperatures on the top surface of the lampshade and the reflector from the open-circuit simulation: (a) one-TEG-chip system, (b) two-TEG-chips system.

simulation result, possibly because of the effect of the metal bolt and nut employed there to fix the heat sink to the reflector which was not simulated. The bolt and nut are closer to the lamp tube than the reflector is, consequently having a higher temperature and thus heating the neighboring reflector. Fig. 11 compares the experimental and simulated open-circuit temperature differences between the hot sides and cold sides of the TEG chips. The experimental temperature differences are inverted from the measured open-circuit voltages. It is observed that the experimental temperature difference of the one-TEG-chip system is close to the simulation result of $k_e = 10$ W/m-K and the average one of the two-TEG-chips system is close to the simulation result of $k_e = 4$ W/m-K. Furthermore, in the two-TEG-chips system the two simulated temperature differences are about the same but the experimental measurements are not. This is because in the simulation a single fiction-fluid region was employed for both TEG chips and the compact heat sink model would homogenize the heat dissipation effect.

Fig. 12 compares the experimentally measured power generation rates with the model predictions as the electric load varies. It is observed that the experimental measurements are slightly lower and more right-skewed than the predictions. We attribute them to the influence of the remaining electric resistance (R_c). By adjusting the value of R_c according to the least square error rule, we find agreement between the predictions and measurements as shown in Fig. 13; the resulting R_c's are 0.78 Ω, 1.59 Ω, and 0.75 Ω respectively for the three systems under investigation.

Furthermore, the 1D model with $R_c = 0\Omega$ predicts a same maximum power generation rate for the series network and the parallel network (see Fig. 12). However, the experimental measurement of the parallel network shows a slightly smaller maximum power generation rate. We attribute this also to the influence of the remaining electric resistance R_c. To highlight it, we calculate the maximum power output from R_{load} for a given R_c and the energy loss (Joule heat) associated with R_c at the corresponding optimal operating current and optimal electric load. Fig. 14 shows the results. Not only the energy loss increases faster but also the maximum power output as well as the total power decreases faster in the parallel network than in the series network as R_c increases. The stronger sensitivity of the parallel network on R_c may be understood by comparing the denominators of Eqs. (5) and (6). Besides, the dependence is not linear due to the nonlinearity associated with Eqs. (1)–(8). In remark, the series network is seemingly preferred since R_c is unavoidable.

4.4. The efficiency of the lamp waste heat recovery

Among the cases investigated herein, the maximum power generation rate is about 1 mW and the waste heat of the lamp is about 10 W. Therefore, the waste heat recovery efficiency is as small as 0.01% although the temperature difference between the heat source (the lamp tubes) and the ambient air is as high as 86 K. Through a detailed examination, we find the low efficiency is mainly caused by the low thermal conductance between the heat source and the hot sides of the TEG chips (K_H). Effort should be made in increasing K_H in order to improve the efficiency, for instance decreasing the distance between the lamp tube and the reflector or replacing the air between the lamp tube and the

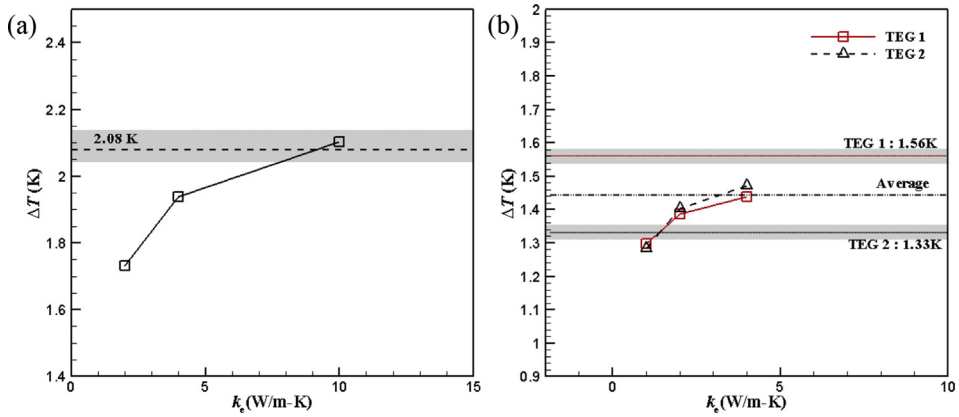

Fig. 11. The temperature differences across the TEG chips against k_e in the open-circuit simulations. The gray regions are the regions experimental data is scattered. (a) one-TEG-chip system, (b) two-TEG-chips system.

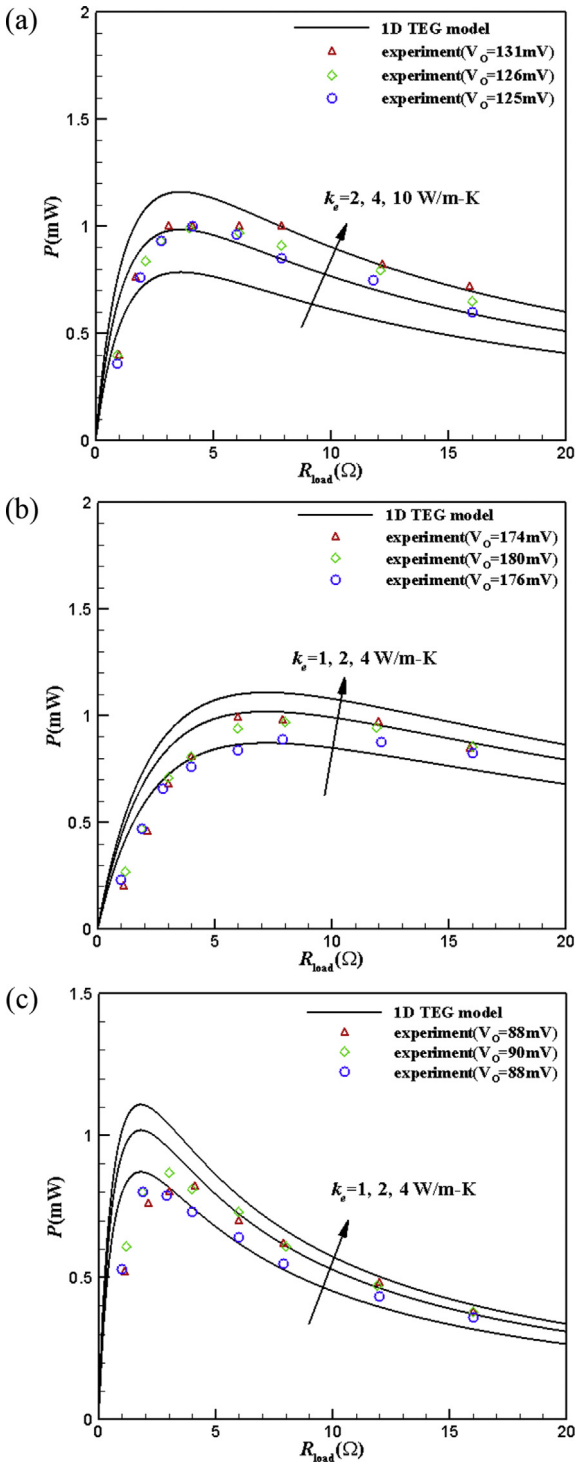

Fig. 12. The measured/predicted power generation rates of the lamp energy recovery systems against the electric load. (a) one TEG chip mounted, (b) two TEG chips connected electrically in series, and (c) two TEG chips connected electrically in parallel.

reflector by some good thermal conductor, as long as the illumination is not affected. On the other hand, a passive heat sink with heat pipes or vapor chamber may be used to increase the heat dissipation effect (i.e. to increase K_C). The thermal management methods of the LEDs introduced by Ye et al. [29] may be applied to the lamp-TEG system. So are the LED lamp cooling apparatus with pulsating heat pipes designed by Chang et al. [30] and the water-cooled-heat-sink assemblies proposed by Rubén [5].

5. Conclusion

In this work, a TEG system for recovering waste heat from the table lamp was attempted. By modeling the Peltier and Joule heats as heat source/sink, we were able to perform closed-circuit simulations in spite of the requirement of an iteration for a converged consistent temperature difference and the induced electric current.

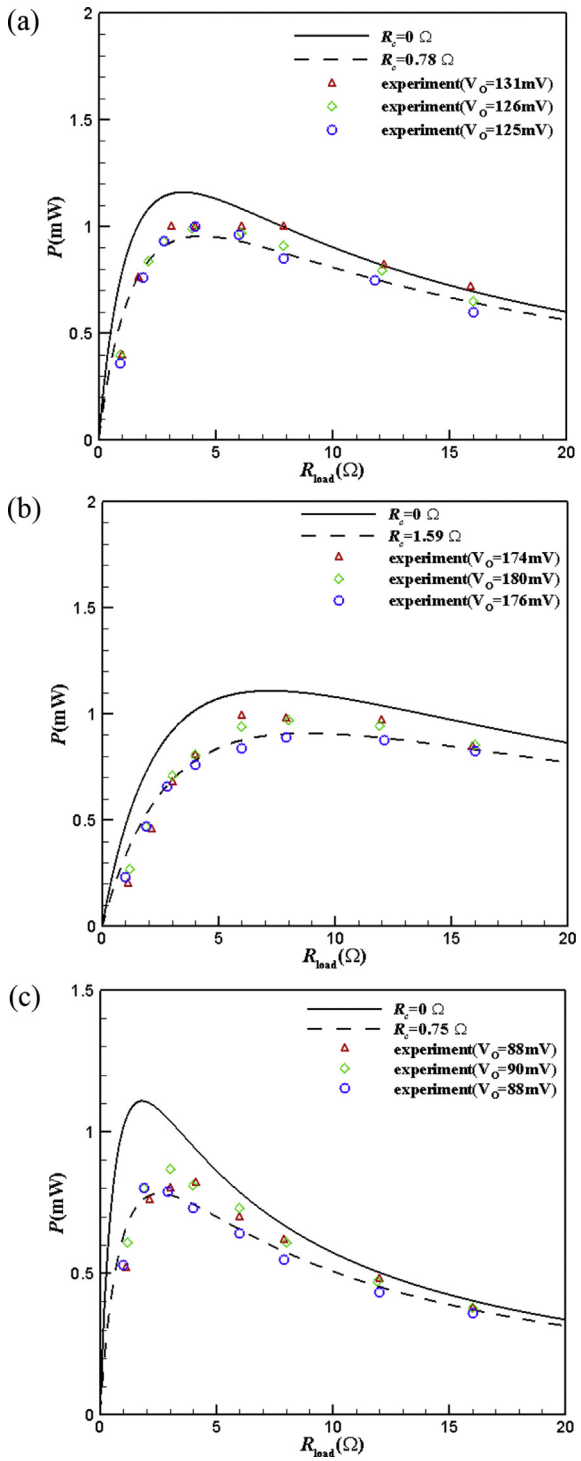

Fig. 13. The measured/predicted power generation rates with zero (solid) and non-zero (dash) R_c. (a) one TEG chip mounted and k_e = 10 W/m-K, (b) two TEG chips connected electrically in series and k_e = 4 W/m-K, (c) two TEG chips connected electrically in parallel and k_e = 4 W/m-K.

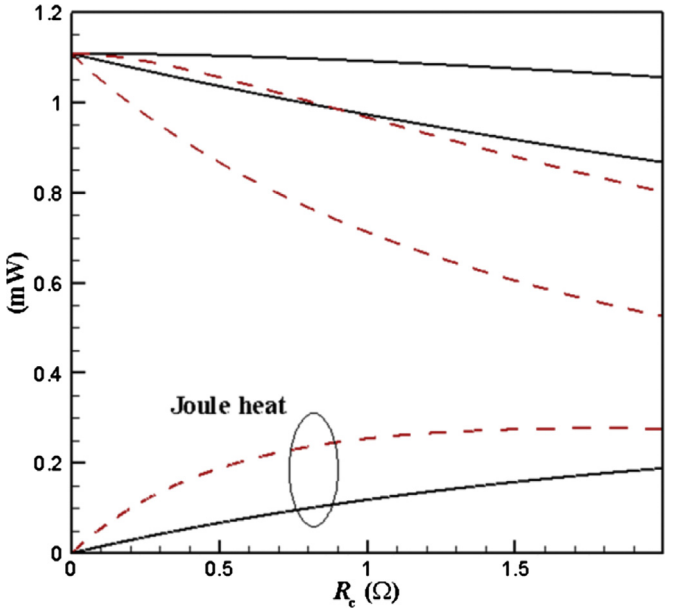

Fig. 14. The generation rates of the Joule heat associated with R_c, the maximum power output via R_{load}, and the total power (the sum of the former two) predicted from the 1D model based on the open-circuit simulation data with k_e = 4 W/m-K and the electric load (R_{load}) optimized (the power output via R_{load} maximized) for each given R_c. Solid lines: the series network; dashed lines: the parallel network.

A 1D TEG model was also proposed which is capable of predicting the power generation rate based on the open-circuit simulation results, namely the thermal conductances between the TEG chips and the thermal reservoirs. The predictions agree well with the closed-circuit simulation results and therefore closed-circuit simulations become avoidable. On the other hand, the 1D model predicts a slightly larger maximum power generation rate and a slightly lower optimal electric load than the experimental measurements. This is attributed to the influence of the remaining electric resistance in the electric circuit. A same reason is employed to explain a lower maximum power generation rate measured in the parallel network than in the series network. Finally, the power generation rate of the current design is as small as 1 mW. The small thermal conductance between the lamp tubes and the TEG chips takes most of the responsibility.

Acknowledgment

This work was supported by the National Science Council of Taiwan (Grant No. NSC 100-2221-E-002 -143 -MY3).

References

[1] Hoboken NJ. Electrical energy efficiency: technologies and applications. Wiley; 2012.
[2] International Energy Agency. Light's labour's lost. Policies for energy-efficient lighting. In support of the G8 plan of action. 2006.
[3] International Energy Agency. Barriers to technology diffusion: the case of compact fluorescent lamps. 2006.
[4] Qin YX, Lin DY, Hui SYR. A simple method for comparative study on the thermal performance of light emitting diodes (LED) and fluorescent lamps. IEEE Trans Power Electron 2009;24(7):1811–8.
[5] M.F. Rubén. Recovery system of the heat dissipated by luminaires, lamps and led devices. European Patent Application EP 2549179A2. 2013.
[6] Saqr KM, Musa MN. Critical review of thermoelectrics in modern power generation applications. Therm Sci 2009;13:165–74.
[7] Leonov V, Vullers RJM. Wearable thermoelectric generators for body-powered devices. J Electron Mater 2009;38:1491–8.
[8] Matsumiya M, Qiu F, Shin W, Izu N, Matsubara I, Murayama N, et al. Thermoelectric CO gas sensor using thin-film catalyst of Au and Co_3O_4. J Electrochem Soc 2004;151:H7–10.
[9] Champier D, Bédécarrats JP, Kousksou T, Rivaletto M, Strub F, Pignolet P. Study of a TE (thermoelectric) generator incorporated in a multifunction wood stove. Energy 2011;36:1518–26.
[10] Hsu CT, Huang GY, Chu HS, Yu B, Yao DJ. Experiments and simulations on low-temperature waste heat harvesting system by thermoelectric power generators. Appl Energy 2011;88:1291–7.
[11] Weng CC, Huang MJ. A simulation study of automotive waste heat recovery using a thermoelectric power generator. Int J Therm Sci 2013;71:302–9.
[12] Suter C, Jovanovic ZR, Steinfeld A. A 1 kW_e thermoelectric stack for geothermal power generation—Modeling and geometrical optimization. Appl Energy 2012;99:379–85.
[13] Chen J. Thermodynamic analysis of a solar-driven thermoelectric generator. J Appl Phys 1996;79:2717–21.
[14] Liang GW, Zhou JM, Huang XZ. Output characteristics analysis of thermoelectric generator based on accurate numerical model. In: Proc. 2nd Int. Conf. on Asia-Pacific Power and Energy Engineering, Chengdu; 2010.
[15] Liang GW, Zhou JM, Huang XZ. Analytical model of series semiconductor thermoelectric generators. J Jiangsu Univ Sci Technol 2011;32:314–9.
[16] Liang GW, Zhou JM, Huang XZ. Analytical model of parallel thermoelectric generator. Appl Energy 2011;88:5193–9.
[17] Astrain D, Vián JG, Martínez A, Rodríguez A. Study of the influence of heat exchangers' thermal resistances on a thermoelectric generation system. Energy 2010;35:602–10.
[18] Antonova EE, Looman DC. Finite elements for thermoelectric device analysis in ANSYS. In: Proc. 24th Int. Conf. on Thermoelectrics, Clemsom, South Carolina, USA; 2005. p. 200–3.
[19] Chen M, Rosendahl LA, Condra T. A three-dimensional numerical model of thermoelectric generators in fluid power systems. Int J Heat Mass Transf 2011;54:345–55.
[20] D.L. Simon, J. Ivey, J.R. Scapa. LED light with thermoelectric generator. US Patent 0234107A1. 2011.
[21] Kajikawa T, Onishi T. Development for advanced thermoelectric conversion systems. In: Proc. 26th Int. Conf. on Thermoelectrics, Jeju, Korea; 2007. p. 322.
[22] http://www.matbase.com/material-categories/.
[23] Narasimhan S, Majdalani J. Characterization of compact heat sink models in natural convection. IEEE Trans Compon Packag Technol 2002;25:78–86.
[24] Narasimhan S, Majdalani J. Compact heat sink simulations in both forced and natural convection flows. In: Proc. 8th AIAA/ASME Joint Thermophysics and Heat Transfer Conf; 2002. St Louis, MO.
[25] Brucker KA, Majdalani J. Equivalent thermal conductivity for compact heat sink models based on the Churchill and Chu correlation. IEEE Trans Compon Packag Technol 2003;26:158–64.
[26] Brucker KA, Majdalani J. Effective thermal conductivity of common geometric shapes. Int J Heat Mass Transf 2005;48:4779–96.
[27] ANSYS, Inc. ANSYS FLUENT 12.0 theory guide. 2009.
[28] Cengel YA. Heat and mass transfer: a practical approach. 3rd ed. New York: McGraw-Hill; 2006.
[29] Ye H, Koh S, van Zeijl H, Gielen AWJ, Zhang GQ. A review of passive thermal management of LED module. J Semicond 2011;32(1–4):014008.
[30] C.S. Chang, J.K. Liu, C.H. Wang, and H.S. Pei. LED lamp cooling apparatus with pulsating heat pipe. US patent 7547124B2. 2009.